

RESEARCH

Open Access



Geomorphic changes after the 2021 Central European flood in the Ahr Valley by LiDAR-based differences

Vanessa Steinritz^{1*}, Piero Bellanova¹, Bernd Schmidt², Holger Schüttrumpf³, Jan Schwarzbauer⁴ and Klaus Reicherter¹

Abstract

Background In July 2021, destructive floods in Western Europe were triggered by enormous precipitation rates related to a low-pressure system named "Bernd." These catastrophic events led not only to major damage to infrastructure, severe economic losses, and the loss of lives but also to significant landscape changes and modifications. Here, we focus, as a case study, on the flood aftermath of the Ahr Valley in Rhineland-Palatinate state in western Germany, as it was one of the most affected and destroyed regions by the flood. We utilize high-resolution Digital Terrain Models (DTMs) based on airborne Light Detection and Ranging (LiDAR) that were taken shortly before and after the flood to investigate insights into geomorphic changes.

Results By calculating Digital Terrain Models of Difference (DoD), we are able to quantify volumetric and areal changes caused by erosional and depositional processes for different sites in the Ahr Valley. Due to the morphology of the narrow Ahr Valley, most of the erosion and deposition is located within the deeply incised canyon of the Ahr River. The comprehensive analysis reveals notable morphological modifications throughout the study area, with a calculated erosion/deposition areal ratio of 0.46 and an erosion/deposition volumetric ratio of 0.63. Our findings indicate massive deposition regarding both areal and volumetric. We selected six different locations along the Ahr Valley that showcase distinct aspects of flood-induced fluvial morpho-dynamics. Deposition occurred mainly in point bars and downstream of destroyed artificial levees, in a braided river style.

Conclusion Our investigations contribute to an overview and assessment of the morphological response to the destructive flood in the Ahr Valley. The results emphasize the necessity for implementing effective flood management strategies, as most of the urban areas in the Ahr Valley were flooded. Moreover, our results provide valuable insights into the impacted areas, highlighting vulnerable locations for flood-related erosion and deposition. This information could contribute to future mitigation and protection efforts, aiding in the development of comprehensive strategies to minimize the impact of similar events in the future.

Keywords Remote sensing, LiDAR, Digital Elevation Model of Difference (DoD), Geomorphic Change Detection (GCD), Flood erosion

*Correspondence:

Vanessa Steinritz

v.steinritz@nug.rwth-aachen.de

Full list of author information is available at the end of the article



© The Author(s) 2024. **Open Access** This article is licensed under a Creative Commons Attribution 4.0 International License, which permits use, sharing, adaptation, distribution and reproduction in any medium or format, as long as you give appropriate credit to the original author(s) and the source, provide a link to the Creative Commons licence, and indicate if changes were made. The images or other third party material in this article are included in the article's Creative Commons licence, unless indicated otherwise in a credit line to the material. If material is not included in the article's Creative Commons licence and your intended use is not permitted by statutory regulation or exceeds the permitted use, you will need to obtain permission directly from the copyright holder. To view a copy of this licence, visit <http://creativecommons.org/licenses/by/4.0/>.

Background

The 2021 Central European floods are a recent reminder of the risk posed by high precipitation flood events with rapidly fast-rising water levels and their catastrophic impact. Between July 12 and 15, 2021, a meteorological constellation prevailed in Central Europe with warm and humid Mediterranean air masses rotated around the low-pressure system "Bernd." The system was locked above Central Europe [1] by the immobile high-pressure area "Cornelieke" in Northeastern Europe [2]. This blockage of the low-pressure system from moving eastwards in combination with orographic effects of the Central European mountain ranges (e.g., Eifel, Ardennes) resulted in persistent extreme precipitation (>150 mm/m²; [3]) for 48 h over Belgium, Luxembourg, the Netherlands, and Germany [1]. The weeks prior to the event were characterized by reoccurring rainfall over western and central Europe, leading to limited free soil water storage capacities (e.g., 10 mm available in RP (Rhineland-Palatinate) and 75 mm in NRW (North Rhine-Westphalia) water storage capacities; [1]). The most affected regions of the Eifel and Ardennes (up to c. 700 m asl) are topographically characterized by narrow V-shaped valleys with steep slopes and thin soils that make the valley-confined river systems prone to amplifying effects regarding acceleration of water flow and rapid and intense water runoff within the confined river system [4].

The limited soil water storage capacity, and topographic-driven amplifying effects are a precondition for high surface run-offs and fast-rising water levels. Numerous small and medium-sized river systems not only in NRW (e.g., Inde, Vicht, Erft, Rur) and RP (Ahr) but also in Belgium or the Netherlands (Vesdre, Ourthe, and Meuse; Fig. 1A) were affected by extreme flooding with estimated water levels up to 7–8 m [3]. Maximum peak discharge values of c. 500 m³/s and 1000 m³/s were recorded for Müsch and Altenahr, respectively [5]. Notably, the water levels and streamflow values can only be estimated as most stream gauging stations have been damaged or destroyed before peak discharge [5–8].

The floods have left drastic scenes of destruction, and most of the affected population faces the ruins of their economic existence. In addition to the destruction of residential buildings, critical facilities and infrastructure (e.g., hospitals, railways, bridges, and utility networks) were destroyed or were only limited accessible after the flood [9]. Trees and shrubs that have been entrained by the extensive water masses, topographic changes, mobilization and remobilization of sediment and rubble,

and environmental pollution have been observed during and after the flood [7, 10, 11].

The insured losses were estimated to be c. € 7 billion [12], and rebuilding efforts measured at $>€$ 30 billion in Germany alone rendered the 2021 Central European floods one of the most expensive natural disaster in Central European history [7]. The fatalities in all affected regions exceed 200 [13]. Neither the unprecedented amounts of rain nor extreme flooding of the small and medium-sized river systems have been anticipated to this extent, which is comparable to an approximately HQ 1000 [14].

Flood events induced by heavy rainfalls represent a common and highly destructive natural hazard. The Central European Flood in 2021 serves as a recent example of the catastrophic impact on infrastructure, socio-economics, and society in well-developed countries during concentrated massive precipitation events. The extend of resulting destruction and morphological changes caused by erosional and depositional forces are often challenging to assess. The Ahr Valley (RP and NRW, Germany) serves as an excellent case study. Due to environmental amplifying effects (acceleration of water flow and rapid and intense water runoff within the confined river system) and socio-economic aspects, the Ahr Valley was one of the most affected regions by the 2021 Central European flood [9, 15].

Initial field observations, which already started during the flood event, provided estimations of flood impacts and identified morphological changes resulting from erosive high-energy flows [5]. Due to limited access to the affected areas or large-scale destruction, a quantitative analysis of the flood impact based purely on field observations is almost impossible.

Modern remote sensing techniques, like airborne LiDAR or Differential Interferometry Synthetic Aperture Radar (DInSAR), offer valuable tools for comprehensive surveys and fast quantitative analysis in challenging terrains, such as hazardous or impassable areas, and provide enhanced observability of remote, dangerous, or large-scale regions [16]. In post-flood analysis and damage assessment, remote sensing enables a comprehensive examination of water pathways, morphological changes, and structural damage. It is also used to evaluate the effectiveness and adaptability of flood protection measures to provide data on needed mitigation measures against future flood events [17]. Flooding in the region is not unusual [6]. Significant flood events, including those in 1804 and 1910, have been recorded in the past.

A peak discharge in Altenahr during the 1804 flood was estimated at $1600\text{m}^3/\text{s}$, while the 1910 event recorded a peak discharge of $710\text{m}^3/\text{s}$. These values are similar and even higher than the discharge value in 2021 [18, 19]. For comparison, the Ahr River usually maintains an average discharge of $6.95\text{m}^3/\text{s}$ [6]. Also, flood risk maps existed before the 2021 flood [20], including calculations for a 100-year event or an extreme event [14]. Unfortunately they did not consider the past flood disasters in 1804 and 1910 (1000-year event) which were comparable to the flood event in 2021 [14, 19].

This study employs high-resolution Digital Terrain Models (DTMs) derived from airborne Light Detection and Ranging (LiDAR) data to calculate Digital Terrain Models of Difference (DoD) for Geomorphic Changes Detection (GCD [21, 22]) as a result of the 2021 Central European floods, explicitly focusing on the Ahr Valley region (Fig. 1). The application of the DoD method in fluvial geomorphology is widely used to evaluate the area and volume of erosion and deposition, estimate river bed level trends, and manage gravel extraction and replenishment [23–26]. In the context of flood analysis for the Ahr Valley, the DoD approach was applied to visualize and analyze flood-related fluvial geomorphic changes across the entire region and quantify the volumetric sediment budget associated with the flood event. Additionally to this analysis, we focused on six specific sites within the valley, each selected to highlight different facets of flood impacts.

Regional setting

The Ahr Valley is situated in the German federal states of NRW and RP (Fig. 1). Tourism due to several natural reserves, viticulture, and cultural-historical aspects is the driving economic force in the Ahr Valley [26, 27]. The region has a prevailing Western European-Atlantic climate. Due to an elevation range of c. 300 m along the river course, the region has slight variations in annual precipitation and temperature from the river spring, located near Blankenheim at 474 m asl (724 mm/yr and $8.0\text{ }^\circ\text{C}$ [28, 29]), to the confluence with the Rhine River (Fig. 1C; [30]), located near Remagen at 53 m asl (671 mm/yr and $10.5\text{ }^\circ\text{C}$ [28, 29]). The Ahr Valley is estimated to have an average annual precipitation of about 675 mm/yr [31].

The Ahr River extends a length of 85.1 km; the Ahr Valley covers an area of 86 km^2 [30] with a catchment area of 897.5 km^2 [18, 32]. It runs through the Rhenish Massif, passing mainly through Devonian units [32, 33] consisting of clay-, silt-, and sandstones of the Klerf, Ulmen, and Vallendar Formations (Early Emsian), clay- and siltstones of the Herford Formation (Late Siegen) [34].

Area 1, located near Antweiler (Figs. 1 and 2), has been chosen to investigate the effects of flooding in areas where the river course is confined. Steep slope flanks, primarily composed of alternating clay-, silt-, and sandstone strata [33], characterize the topography beside the riverbed, exhibiting angles ranging from about 22° to 40° . Here, the river meanders pass through a narrow channel (c. 40 m width), flanked by steep slopes to the south and elevated terrain to the north (Fig. 2A). Downstream, the width of the valley increases to c. 230 m after a turn of the course to the north.

We introduce the relatively wide open floodplain in Dümpelfeld as Area 2. The valley is bound by steep slope flanks (30° up to max. 50°) composed of alternating strata of clay-, silt-, and sandstones of the Middle Siegen formation [34]. The area within the valley was almost entirely flooded by the river, among which also the sewage treatment plant of Dümpelfeld was flooded and destroyed (Fig. 3B, C).

Area 3, situated near Brück, has been chosen for its exemplary flood impact effects on the geomorphology of an incised narrow valley-confined river loop (Fig. 4). In this region, the riverbed is confined and bordered by steep slopes, with angles reaching approximately 30° (up to max. 50°), predominately consisting of alternating strata of clay-, silt-, and sandstones of the Middle Siegen (Pragium) [34].

Area 4 was selected for its distinctive topographical characteristics (Fig. 5). By considering elevation data (Fig. 1), within this region, the Ahr Valley undergoes a notable morphological transition from a relatively narrow valley upstream to the west (c. 60 m) to a wider valley (c. 200 m) downstream toward the east (Fig. 5). The valley flanking topography in this area shows steep slope (up to 30°), predominately consisting of alternating strata of clay-, silt-, and sandstones of the Middle Siegen [34].

Area 5 in Ahrweiler was chosen as it marks a highly urbanized environment along the river course (Fig. 6).

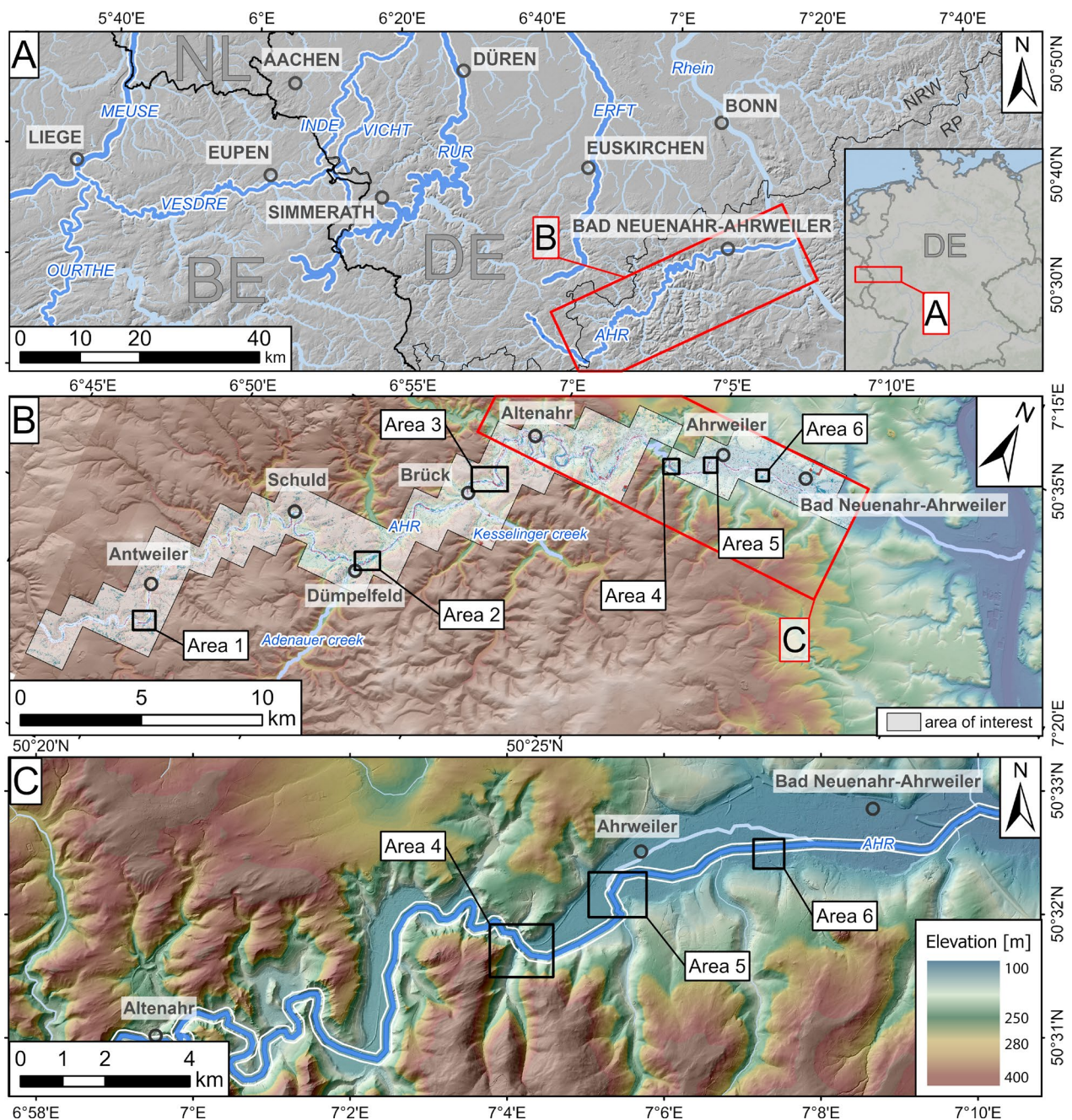


Fig. 1 **A** Main river systems affected by the flood in 2021; DE: Germany, BE: Belgium, NL: the Netherlands; red rectangle refers to **B**. **B** Overview map of the Ahr Valley with elevation changes from DTM of Difference (DoD) and in details studied subareas (black rectangle); red rectangle refers to **C**. **C** Distinction of topographical features and elevation between narrow valley-confined and broader valley river section near the confluence of the rivers Ahr and Rhine

Area 6 was chosen for its exemplary feature of a temporary depositional site (Fig. 7).

Methods

High-resolution airborne Light Detection And Ranging (LiDAR, ALS) data were recorded in the study area of the Ahr valley prior (2019/2020) and after (Aug. 2021) the 2021 Central European flood. The pre- and post-flood LiDAR data cover an area of $\sim 84 \text{ km}^2$ (Fig. 1B). They

were recorded using airborne LiDAR scanner Riegl LMS Q780 and Riegl LMS VQ780 II with an average point density of 25 points/m² for 2019/2020 and 66 points/m² for 2021. The aerial surveys were conducted as part of the routine annual schedule and as well as an additional flight after the flood in 2021, to capture and re-scan various areas within Rhineland-Palatinate. Data processing was archived by the client, LVerGeo. Consequently, the datasets utilized in our study were provided by LVerGeo, and we strictly adhered to the original data specifications and parameters, including coordinates, resolution, ground control points (tree control areas), point cloud density (25 points/m² and 66 points/m²), and the conversion process to Digital Elevation Models (DEM) or Digital Terrain Models (DTM) (resolution of 0.2 m). Our analysis was based solely on the supplied datasets, maintaining their integrity without any technical alterations or modifications. By superposition and differentiating the provided pre- and post-flood DTMs of the Ahr Valley with a resolution of 0.2 m, a DTM of Difference (DoD) was calculated for Geomorphic Change Detection (GCD) after Williams [23]:

$$\delta E = Z_2 - Z_1. \quad (1)$$

Here, δE represents the elevation changes in the resulting DTM, and Z_1 corresponds to the elevation values of the pre-flood DTM and Z_2 to the elevation values of post-flood DTM [23]. Calculations were conducted using the geographic information system of Esri ArcGIS (Version 10.7.1). We used the internal Raster Calculator which allows to perform mathematical operations on multiple raster data. It enables the creation of new raster datasets based on the calculations applied to the input raster layers. The raster calculator operates on a cell-by-cell basis, applying the specified mathematical expressions or functions to the corresponding cells of the input rasters. The data in our study are referred to the coordinate System ETRS 1989 UTM Zone 32N.

The resulting DoD encompasses information regarding the elevation change between pre- and post-flood data for each raster pixel. Positive values within the DoD indicate a positive topographic change, i.e., a gain in elevation, which is interpreted as deposition, whereas negative values specify a negative topographic change, i.e., a loss in elevation, which is interpreted as erosion. This information enables the quantification of the areal extent and volumetric dimension of geomorphic changes. However, sometimes the process behind the origin of deposition or erosion is not clear and can be anthropogenic. We refer to "deposition" and "erosion" in the following for easier understanding.

The computation of volume for each raster cell involves multiplying the area [m²] of the raster cell (0.2 m × 0.2 m) by the corresponding elevation change information from the DoD. The quantification of deposition and erosion volume across the entire area can be derived by aggregating the respective values.

To mitigate potential misinterpretation in the DoD of small change values associated with annual changes in the DTM (e.g., by vegetation (not the tree/shrub growth but soil thickness changes by leaves deposited), minor landscape changes, shrinking and swelling of soils in dry or wet summers, or lastly anthropogenic influences), a threshold represented as a technical "minimum Level of Detection ($_{\min}\text{LoD}$)" is conducted after Brasington et al. [35] and Wheaton et al. [25]:

$$U_{\text{crit}} = t \sqrt{\text{SDE}_{\text{new}}^2 + \text{SDE}_{\text{old}}^2}, \quad (2)$$

where U_{crit} is the critical threshold or the $_{\min}\text{LoD}$, t is the "student's t -value" at a chosen confidence interval, and SDE is the standard deviation of elevation from the individual DTM. The information of SDE values for the individual DTM were provided and obtained by 3 control areas by the LVerGeo RLP. In our study, we chose a confidence interval of 95%, which results in $t=1.96$. With an SDE_{new} of 0.026 m and SDE_{old} of 0.028 m, we calculated a $_{\min}\text{LoD}$ of 0.074 m. Due to the fact, that the calculated technical $_{\min}\text{LoD}$ shows a very low value of just 0.074 m and could still lead to a misinterpretation of small DoD values, we deviated from the calculated technical $_{\min}\text{LoD}$. We applied a more conservative $_{\min}\text{LoD}$ of 0.2 m to archive a better approximation of morphological changes excluding annual changes. Values exceeding the $_{\min}\text{LoD}$ of 0.2 m are considered significant, whereby values below are considered as uncertainties and therefore characterize no morphologic changes [23, 25, 35].

We chose six locations along the Ahr Valley (Figs. 1, 2, 4, 5, 6, 7) that represent different aspects of flood dynamics impacts for in-depth analysis: Area 1—Antweiler, which comprises narrow river passages in a narrow valley section (Fig. 2); Area 2—Dümpelfeld, including the confluence of Ahr and the Adenauer creek (Fig. 3); Area 3—Brück, a river loop of the Ahr (Fig. 4); Area 4—Ahrweiler I, landscape change from a narrow to an open more expansive valley (Fig. 5); Area 5—Ahrweiler II, urban environment with anthropogenic modification (Fig. 6); and Area 6—sports field Bachem in Bad Neuenahr-Ahrweiler, urban environments with channelized river sections and anthropogenic modifications (Fig. 7).

Topographic cross-sections perpendicular to the river flow direction are generated in ArcGIS

for pre- and post-flood data to contribute to the visualization of erosion and sedimentation processes responses. In March 2022, aerial imagery using a Phantom 4 Pro Advanced drone was acquired within the Ahr Valley to provide additional image-based insights. We flew the drone for capturing images almost 1 year after the flood, aiming to observe the analyzed changes in the landscape.

Results

The geomorphic change detection (GCD) results reveal that the Ahr Valley and especially the valley floor and river course have undergone significant flood-related morphological changes affecting both area and volume

(Table 1). Of the total area of 84.6 km², approximately 7.4% (6.3 km²) show a positive elevation change (deposition), while 3.4% (2.9 km²) display a negative elevation change (erosion). Thus, an erosion/deposition area ratio of 0.46 results from the data (Table 1). The volumetric change of the area yields c. 3,198,107 m³ of deposition and 2,011,192 m³ erosion, which gives a volumetric erosion/deposition ratio of 0.63 (Table 1). Areal and volumetric changes indicate that sedimentation outweighed erosion in the Ahr Valley during the Central European flood in 2021. Even higher values are given for both erosion and deposition when the LoD is not considered (Table 1).

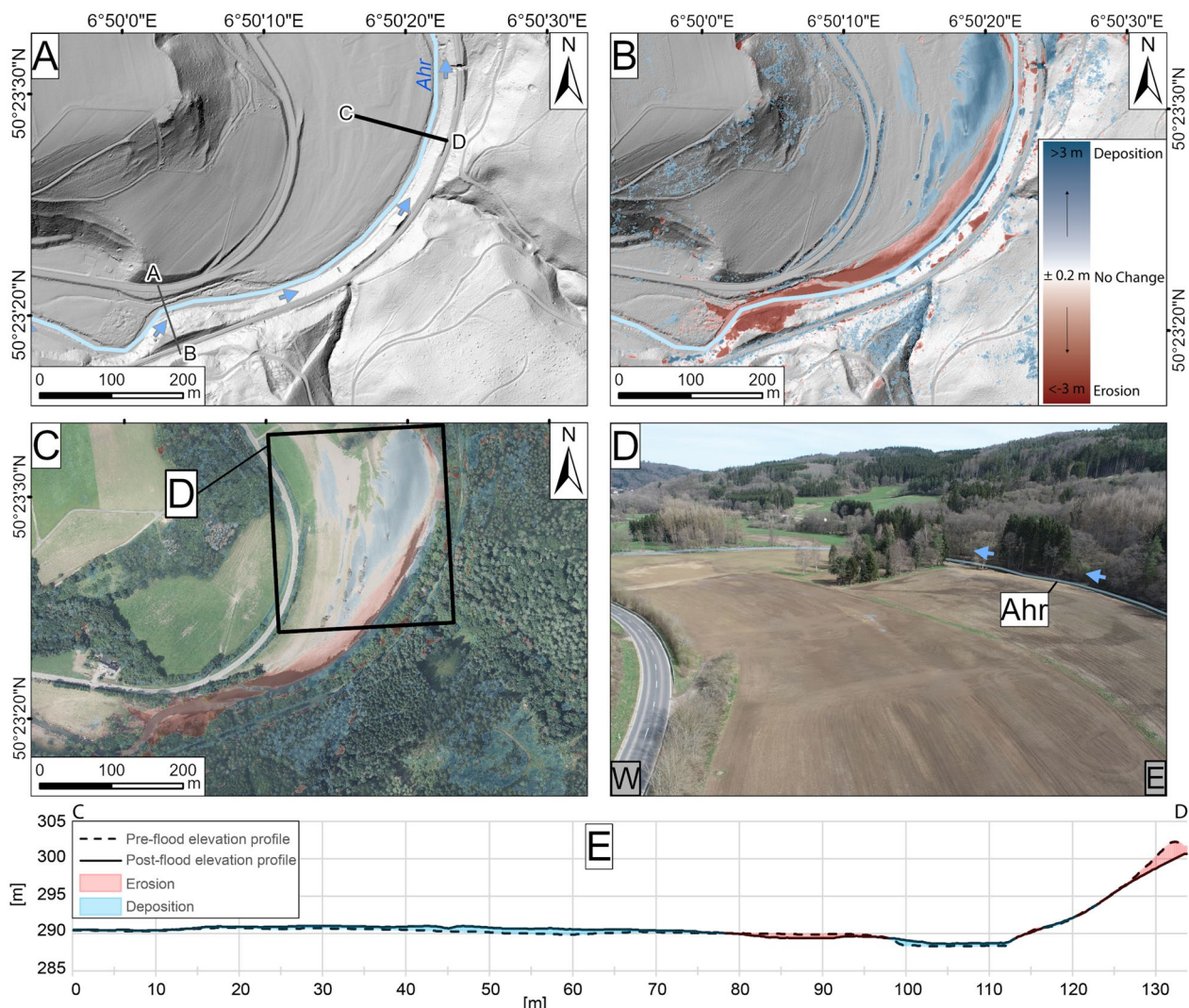


Fig. 2 Area 1—Antweiler. **A** High-resolution (0.2 m) pre-flood DTM with the location of profile lines **B** High-resolution (0.2 m) post-flood DTM and DoD results. **C** Orthophoto taken in 2021 after the flood overlaid by DoD results. **D** Photo of area, taken on April 12, 2022. **E** Cross-section C–D (location shown in **A**) across the Ahr river. For cross-section A, B, see additional file 1 Fig. S1

Area 1—Antweiler

The geomorphic setting of Area 1, characterized by steep slopes restricting the Ahr Valley, acts as a natural confined on the river's ability to expand its course during periods of increased water discharge, such as during the flood event. As a result, the confined space within Area 1 channels the force of the water, leading to heightened erosion along its banks and bed compared to areas with more expansive channels. Erosion values of up to 5 m is observed here. This erosion affected agricultural and forest areas, partly collapsed levee flanks, road dam failure, and sliding mountain slopes due to the increased water discharge, erosion, and associated water pressure.

Conversely, depositional patterns were observed downstream toward the north, albeit at a lower value (~ 1 m). Here, the river course encounters gentle slopes

and elevated terrains on one side. The flood plain offers the space and leads to a flow speed reduction and, hence, to deposition (Fig. 2B, C). Data from Area 1 reveal a significantly larger deposition area ($52,496 \text{ m}^2$) and larger volumes ($23,900 \text{ m}^3$) than erosion area ($23,645 \text{ m}^2$) and volume ($-20,079 \text{ m}^3$) (Table 2). The forested slopes indicate a diffuse pattern of deposition (blue), which could not clearly be interpreted in term of the process behind. It could be due to slide masses or DTM accuracy.

Area 2—Dümpelfeld

In Dümpelfeld (Area 2), we examine the flood-induced morphological alterations in the specific environment downstream of confluences (Fig. 3). Here, in Dümpelfeld the confluence of the Adenauer creek and Ahr river

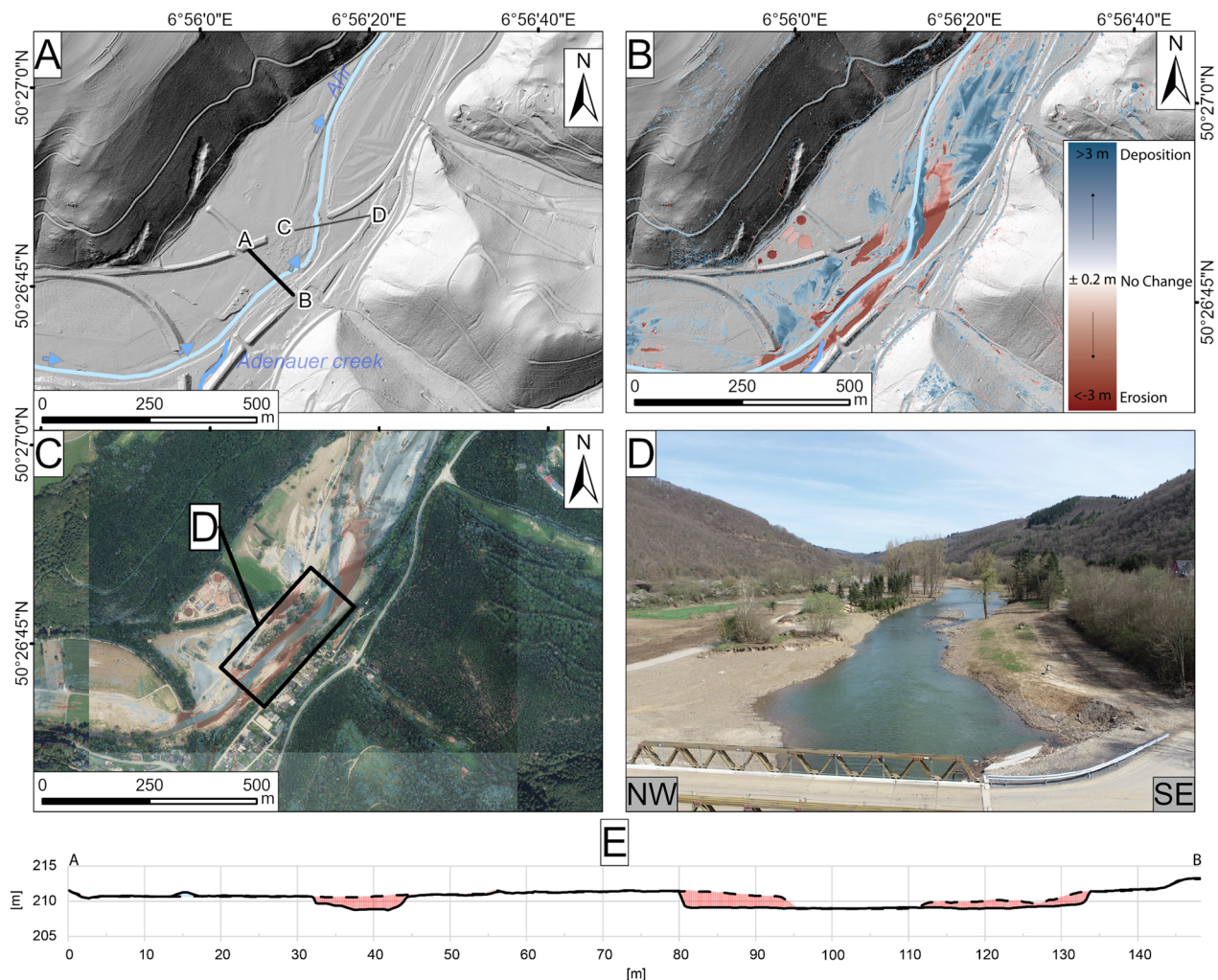


Fig. 3 Area 2—Dümpelfeld. **A** High-resolution (0.2 m) pre-flood DTM with the location of profile lines. **B** High-resolution (0.2 m) post-flood DTM and DoD results. **C** Orthophoto taken in 2021 after the flood overlaid by DoD results. **D** Photo of area, taken on April 12, 2022. **E** Cross-section A–B (location shown in **A**) across the Ahr river. For cross-section C, D, see Additional file 1: Fig. S2

is located. Data from this area indicate a structural failure of a bridge coupled with high erosion values (up to 3 m) downstream of this confluence (Fig. 3B–D). Besides erosion, depositional areas are observed further downstream where the river has sufficient space within the flood plain to propagate and was able to overtop the banks without blockage. The river developed from a gently meandering to a braided river (Fig. 3A, B). The sewage treatment plant in Dümpelfeld was protected by two dikes, one of which is an ancient railway dam. Obviously, they could not prevent the destruction of the plant. Area 2 generally shows a larger deposition area (138,921 m²) than erosion area (52,258 m²) as well as a

higher volume of deposition (65,004 m³) than erosion volume (42,170 m³) (Table 2).

The bridge failure and large erosion values can be attributed to an accumulation of debris in front of the bridge. It obstructed the narrow bridge passages and led to a water flow blockage. As a result, the dammed water sought alternative pathways, leading to substantial erosion and deposition, such as downstream crevasse splay deposits (Fig. 3B). The high hydraulic pressure exerted upon the bridge finally led to a collapse. About 75% of the bridges along the valley show damage, with approximately half of them destroyed during the flood in 2021 [36].

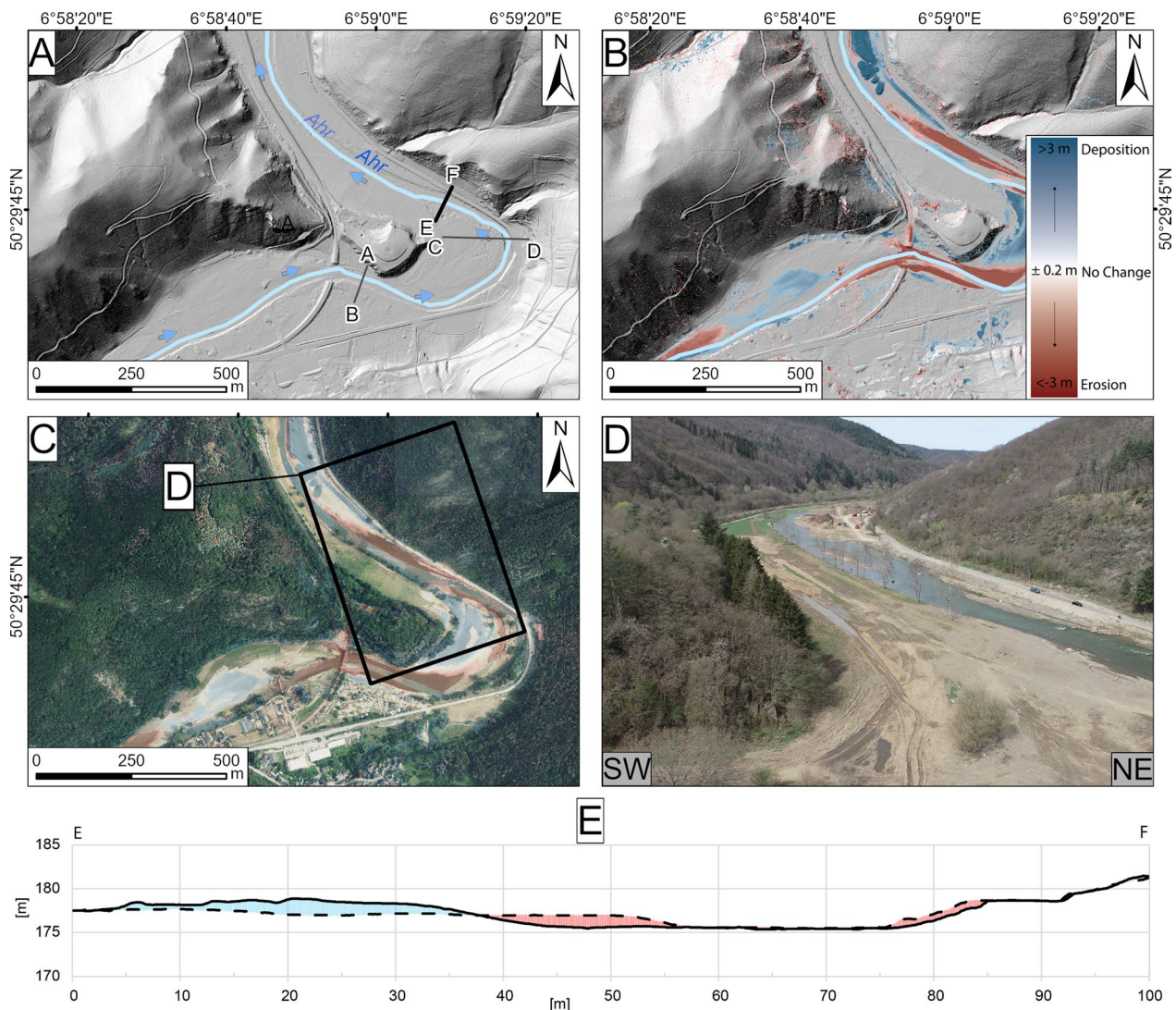


Fig. 4 Area 3—Brück. **A** High-resolution (0.2 m) pre-flood DTM with the location of profile lines **B** High-resolution (0.2 m) post-flood DTM and DoD results. **C** Orthophoto taken in 2021 after the flood overlaid by DoD results. **D** Photo of area, taken on April 12, 2022. **E** Cross-section E-F (location shown in **A**) across the Ahr river. For cross-sections A–B and C–D, see Additional file 1: Figs. S3 and S4

Area 3—Brück

Intense erosion occurs at the river's cliffside in the valley of Area 3 by scouring, whereas overbank deposition occurred at the slip-off slope (Fig. 4B, C). In the northern course of the river, flood debris and sediments were piled up to 4 m height during the clean-up works immediately after the flood; these deposits are considered as anthropogenic. Furthermore, a comparable situation as in Area 2 can be observed, characterized by structural bridge failures coupled with intense erosion by scouring.

As described in Area 2, the recurring scenario in Area 3 involves debris obstructing the bridge passageways, leading to structural failures and the formation of alternative waterways, consequently contributing to substantial erosion (Fig. 4B–D). In general, this area exhibits a larger areal erosion ($95,097 \text{ m}^2$) in contrast to the depositional area ($87,881 \text{ m}^2$) as well as a larger erosion volume ($61,824 \text{ m}^3$) compared to the depositional volume ($57,009 \text{ m}^3$) (Table 2).

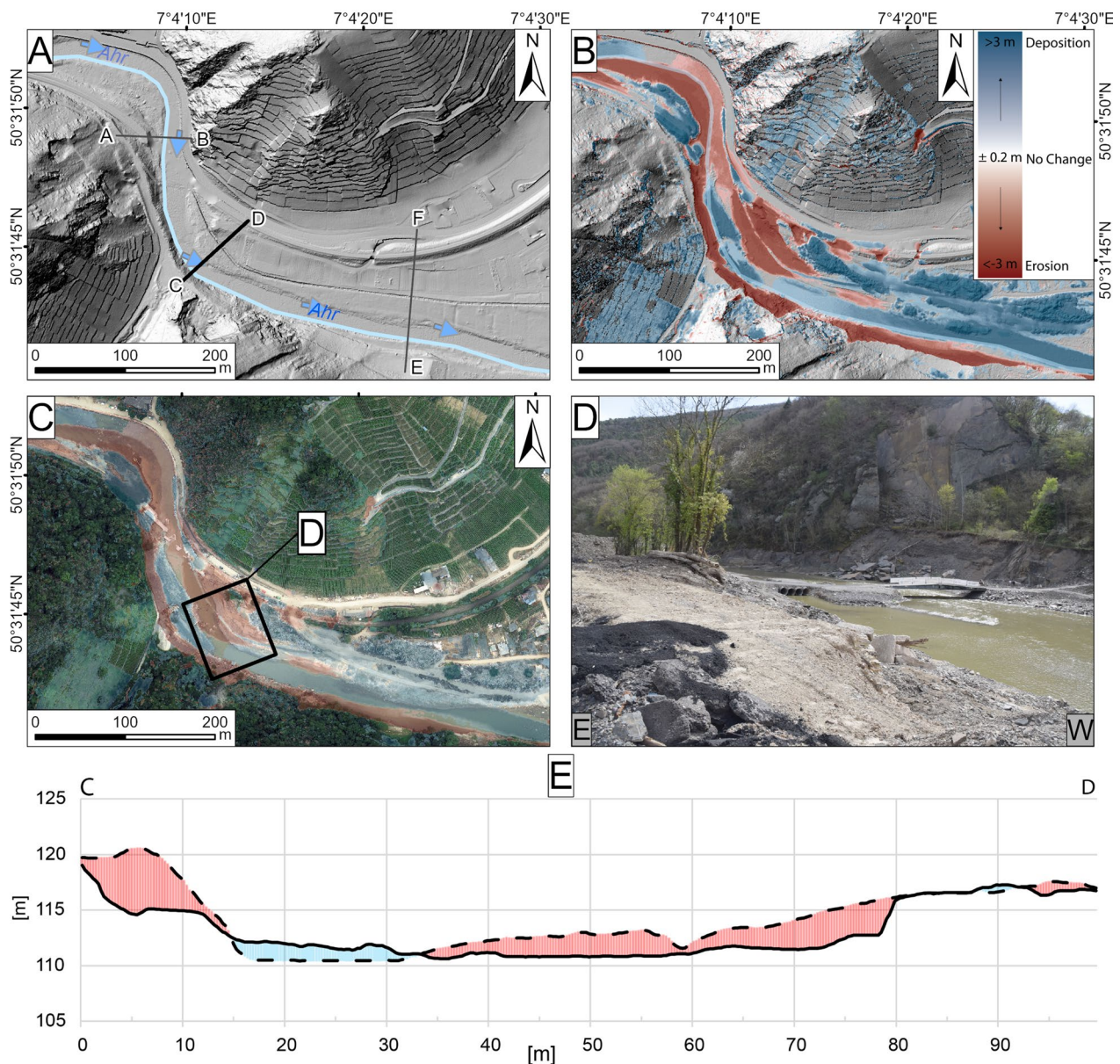


Fig. 5 Area 4—Ahrweiler I. **A** High-resolution (0.2 m) pre-flood DTM with the location of profile lines. **B** High-resolution (0.2 m) post-flood DTM and DoD results. **C** Orthophoto taken in 2021 after the flood overlaid by DoD results. **D** Photo of area, taken on April 12, 2022. **E** Cross-section C–D (location shown in **A**) across the Ahr river. For cross-sections A, B and E, F, see Additional file 1: Figs. S5 and S6

Area 4—Ahrweiler I

During the flood event, the riverbed expanded in Area 4 from c. 2.2 m to 30 m in width (Fig. 5A, B). The morphologic situation to the west forced the high discharge river to channelize, resulting in high erosion values up to 4 m by scouring, where flanks partly collapsed. Moreover, a comparable scenario, as in Areas 2 and 3, concerning amplifying erosive effects by bridge blocking and failure can also be observed here (Fig. 5B–D). Conversely, as the valley opens up toward the east, the river benefits from increased space for its flow, resulting in a reduction of water velocity and subsequent higher deposition. Additionally, as described in Area 3, flood debris and sediments were piled up here to 5 m height during the clean-up works immediately after

the flood. In general, a significantly larger deposition area ($65,786 \text{ m}^2$) can be observed in Area 4 than the erosion area ($29,770 \text{ m}^2$), as well as a larger deposition volume ($53,293 \text{ m}^3$) than the erosion volume ($39,291 \text{ m}^3$) (Table 2).

Area 5—Ahrweiler II

The data in Area 5 reveal anthropogenic depositional piles of up to 5 m height and erosion of up to 3 m. During the flood, the riverbed expanded from its usual width of c. 14 m to c. 57 m, resulting in the inundation of urban areas, including housing and infrastructure (e.g., streets, destruction of bridges, etc.) (Fig. 6). The data depict a larger erosion area ($28,936 \text{ m}^2$) than deposition area ($20,652 \text{ m}^2$) and a smaller depositional

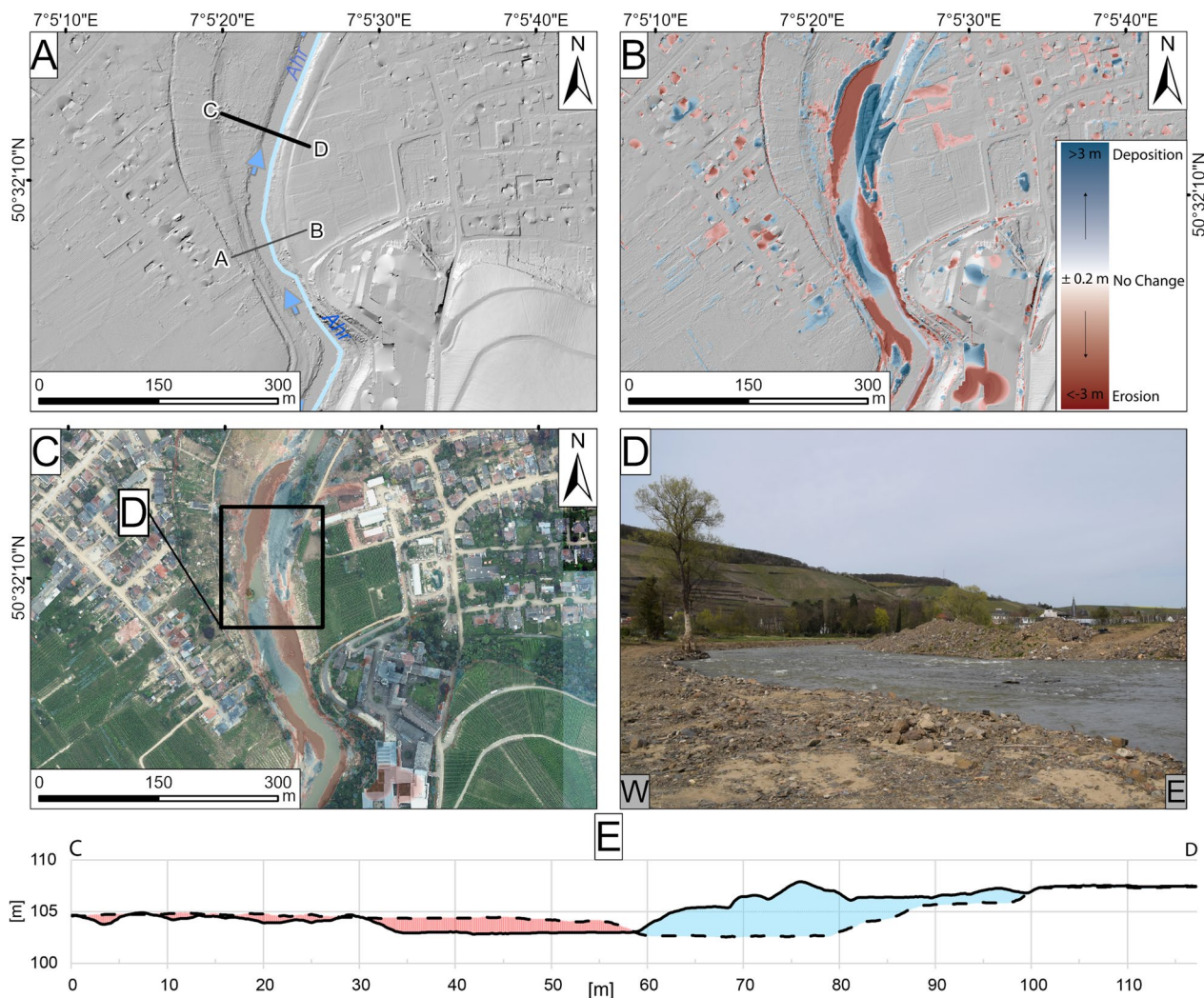


Fig. 6 Area 5—Ahrweiler II. **A** High-resolution (0.2 m) pre-flood DTM with the location of profile lines. **B** High-resolution (0.2 m) post-flood DTM and DoD results. **C** Orthophoto taken in 2021 after the flood overlaid by DoD results. **D** Photo of the area, taken on April 12, 2022. **E** Cross-section C–D (location shown in **A**) across the Ahr River. For cross-section A–B see additional file 1: Fig. S7

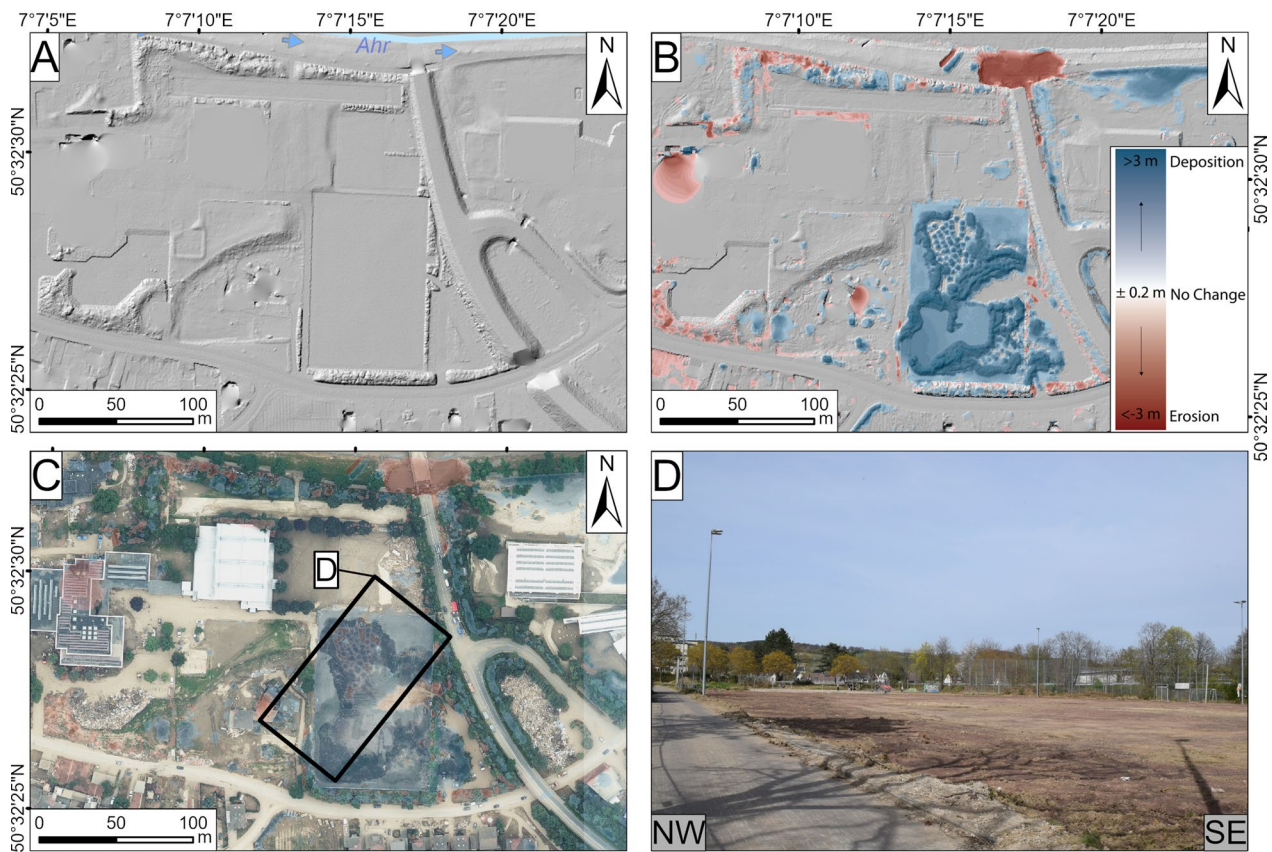


Fig. 7 Area 6—Sports field Bachem in Bad Neuenahr-Ahrweiler. **A** High-resolution (0.2 m) pre-flood DTM. **B** High-resolution (0.2 m) post-flood DTM and DoD results. **C** Orthophoto taken in 2021 after the flood overlaid by DoD results. **D** Photo of area, taken on April 12, 2022

Table 1 Calculated values for areal coverage in [m²], volumes in [m³], erosion (E) and deposition (D) ratios for areal coverage (A) and volume (V), and the net surface changes for areal coverage and volume for the entire study area

minLoD [cm]	Area [km ²]		Area [%]		E _A /D _A	Net change area [km ²]	Volume [m ³]		E _V /D _V	Net change volume [m ³]
	Erosion	Deposition	Erosion	Deposition			Erosion	Deposition		
–	33.5	41.7	39.6	49.3	0.80	8.2	3,764,741	5,537,999	0.68	1,773,258
7.4	11.4	18.7	13.5	22.1	0.61	7.3	2,992,235	4,725,700	0.63	1,733,465
20	2.9	6.3	3.4	7.4	0.46	3.4	2,011,192	3,198,107	0.63	1,186,915

Results are presented for three considerations of a minimum Level of Detection (minLoD) = threshold, which are no minLoD, the calculated technical minLoD of 7.4 cm, and the conservative assumed minLoD of 20 cm

volume (18,278 m³) than the erosion volume (24,497 m³) (Table 2).

Area 6—Sports field Bachem in Bad Neuenahr-Ahrweiler

The Area 6 covers the sports field Bachem, where flood debris material was temporarily dumped after the flood. A depositional pile elevation of about 3 m was calculated from the LiDAR data. Additional file 1: Fig. S1D shows that the sports field was already cleared on April 12, 2022 of the anthropogenic dump deposits. High erosion can

be seen in the northern part of the area. An orthophoto interpretation (Fig. 7C) suggests that the collapse of a nearby bridge could have caused this erosion by blockage and underflow, as seen in Areas 2–4 (Fig. 7B–D). The data reveal a larger deposition area (16,131 m²) than the erosion area (7,205 m²) and a higher deposition volume (12,197 m³) than the erosion volume (4888 m³) (Table 2).

Table 2 The table displays calculated values for areal coverage in [m²], volumes in [m³], erosion (E) and deposition (D) ratios for areal coverage (A) and volume (V), and the net surface changes for areal coverage and volume for all subareas.

Area	minLoD [cm]	Area [m ²]		E _A /D _A	Net change Area [m ²]	Volume [m ³]		E _V /D _V	Net change Volume[m ³]
		Erosion	Deposition			Erosion	Deposition		
1	–	95,855	226,963	0.42	131,108	24,030	36,915	0.65	12,885
	7.4	42,257	126,066	0.34	83,809	22,354	33,371	0.67	11,017
	20	23,645	52,496	0.45	28,851	20,079	23,900	0.84	3,821
2	–	324,165	796,430	0.41	472,265	59,230	112,060	0.53	52,830
	7.4	140,826	402,021	0.35	261,195	52,866	97,333	0.54	44,467
	20	52,258	138,921	0.38	86,663	42,170	65,004	0.65	22,834
3	–	712,043	352,879	2.02	–359,164	107,795	75,019	1.44	–32,776
	7.4	357,227	183,520	1.95	–173,707	94,117	69,070	1.36	–25,047
	20	95,097	87,881	1.08	–7,216	61,824	57,099	1.08	–4725
4	–	70,819	199,211	0.36	128,392	42,071	63,858	0.66	21,787
	7.4	44,807	128,612	0.35	83,805	41,146	60,842	0.68	19,696
	20	29,770	65,786	0.45	36,016	39,291	53,293	0.74	14,002
5	–	156,178	96,313	1.62	–59,865	31,242	23,070	1.35	–8,172
	7.4	56,837	45,581	1.25	–11,256	27,838	21,362	1.30	–6,476
	20	28,936	20,652	1.40	–8,284	24,497	18,278	1.34	–6,219
6	–	36,796	61,342	0.60	24,546	6,727	15,071	0.45	8,344
	7.4	17,112	31,854	0.54	14,742	6,094	14,157	0.43	8,063
	20	7,205	16,131	0.45	8,926	4,888	12,197	0.40	7,309
x̄	–	232,643	288,856	0.91	56,213	45,183	54,332	0.85	9,149
	7.4	109,844	152,942	0.80	43,098	40,736	49,356	0.83	8,620
	20	39,485	63,645	0.70	24,159	32,125	38,295	0.84	6,170

Results are presented for three considerations of a minimum Level of Detection (minLoD) = threshold, which are no minLoD, the calculated technical minLoD of 7.4 cm, and the conservative assumed minLoD of 20 cm. The average (\bar{x}) values for each characteristic are presented in the last row.

Discussion

Geomorphic Change Detection (GCD) results show significant morphological changes in the Ahr Valley caused by the 2021 flood event. The six selected locations along the Ahr Valley represent the variety of distinct morphological changes due to flood dynamics, including areas with narrow channels, confluences, anthropogenic modifications, and varying topographical characteristics (Figs. 2, 3, 4, 5, 6, 7). The volumetric change of the area yields c. 3 mill. m³ of deposition and 2 mill m³ of erosion. More was deposited than eroded within the Ahr Valley.

Data show that areas of narrow river sections with undercut slopes and confluences experienced enhanced erosional processes, likely due to increased flow velocity, water supply, and turbulence flow (Figs. 2, 3, 4, 5, 6, 7), causing scouring effects. Studies of Anderson and Anderson 2010 and Hjulström 1942 confirm the relationship between flow acceleration and increased erosion rates [37, 38]. Conversely, areas characterized by low elevation and greater valley width show a higher areal percentage of deposition due to reduced flow velocities [5, 37, 38] (Figs. 2, 3, 4, 5, 6, 7). The reduced energy of the water in these areas leads to the accumulation of material

in the wider valley parts. This process is also observed in river bends, where flow velocity decreases (Figs. 2, 3, 4, 5, 6, 7). Images taken during or in the direct aftermath of the flood show the blockage of bridges resulting in riverbed expansion and alternative waterways which lead to major erosion and further downstream to higher deposition values [5] (Figs. 5,6, 7). The Ahr River exceeded its bankfull stage and nearby urban areas and infrastructure. Erosion along the slopes can be attributed to the effects of water flow during precipitation events. The devastating impact of the 2021 flood event and the extensive morphological alterations in the Ahr Valley emphasizes the necessity for a comprehensive reevaluation of the flood risk management and reconstruction strategies and underlines the need for enhanced flood protection measures, as most of the urban areas in the Ahr Valley were flooded. Our results highlight the vulnerability of the entire areas to flood-induced morphological alterations and could contribute to investigate protection measures for future floods.

The calculation of a DoD in the Ahr Valley has provided valuable insights into erosion and deposition patterns and their resulting dynamics behind it caused by

extensive precipitation during the flood in 2021. The DoD in our study relies on high-resolution LiDAR data, which provides accurate elevation measurements and enables the detection of subtle changes in the terrain. Furthermore, the method enables to quantify volumetric and areal changes. One notable advantage of applying the DoD method in the study area is its ability to capture large-scale and small-scale elevation changes, providing a holistic perspective on the distribution and extent of erosion and deposition in the entire valley and specific sites. This information is vital for understanding the geomorphic response to flood events and can aid in developing effective flood management strategies. It provides the chance to identify vulnerable areas which record a high flood impact. These areas may need special attention in future flood risk management efforts, allowing for the implementation of targeted measures to mitigate the impact of potential future flooding.

Despite its advantages, the applying the DoD approach is not without limitations. The input data quality and resolution significantly influence the accuracy and reliability of the results. The technical threshold of 7.4 cm provided by the recording of the data quantifies a degree of uncertainty. Therefore, detecting minimal changes, particularly in the range of centimeters, constitutes a limitation that should be considered while interpreting the results and considering the magnitude of erosion and deposition values, as we did with a conservative assumption with a minimal Level of Detection of 0.2 m.

Another methodological limitation pertains to filtering anthropogenic influences in the elevation models, such as the presence of houses and infrastructure. While efforts were made to exclude these features, filtering them consistently across the datasets can be challenging. Inaccuracies in the filtering process can introduce uncertainties and impact the calculated erosion and deposition values. Additionally, the results of the DoD do not account for potential sediment composition or grain size variations, which can differently influence the erosional and depositional processes and implies that sediment mass can only be estimated based on the measured volume by assuming a bulk density that is frequently not measured [37, 38]. It is essential to acknowledge that the DoD approach provides a snapshot of the landscape at two specific time points (pre-flood and post-flood). The dynamic nature of erosion and deposition process responses necessitates the consideration of temporal variability. Seasonal influences, sediment supply changes, anthropogenic alterations, and water flow conditions variations can influence the observed erosion and deposition patterns. Besides temporary variabilities, hollow spaces beneath deposition, as well as

deposition in facilities, should be considered potential sources of miscalculations. This is particularly relevant in anthropogenic rubble heaps where voids or hollow spaces may exist due to the nature of the materials and the deposition process. While natural sediment deposits may not typically exhibit hollow spaces, rapid deposition, including entrained trees and other vegetation, as well as rubble, during the flood event could introduce some hollow spaces even in natural deposition. The extent of the data lacking from those specific sites is almost impossible to estimate using the DoD method and should be considered while interpreting the results.

Lastly, perturbations observed on the slopes need to be checked by the process behind the modification of the land surface (e.g., Figs. 2B or 4B). It is not really clear what process causes the "punctual" or spotty changes of topography, mostly probably uncertainties in the DTMs, as the uncertainties increase with steep slopes or dense vegetation [39].

Despite its limitations, applying the DoD method in this case study has demonstrated utility in capturing and quantifying erosion and deposition dynamics in the Ahr Valley area. It provides a valuable tool for our study site for assessing the geomorphic response to flood events and identifying areas of high vulnerability. By understanding the patterns and processes of erosion and deposition, policymakers and hydraulic and civil engineers can make informed decisions regarding flood risk management, land use planning, and infrastructure development.

Conclusion

Geomorphic Change Detection (GCD) through high-resolution Digital Terrain Model of Difference (DoD) proved to be essential in understanding morphological changes caused by the devastating flood event in 2021 in the Ahr Valley. We obtained an overview of morphological alterations resulting from the flooding on both catchment encompassing and site-specific scales. Moreover, it enabled an approximate quantitative estimation of volumetric and areal changes, particularly advantageous in inaccessible and large terrains. Six specific locations along the Ahr Valley further demonstrated diverse morphological responses to the substantial flood event, such as intensifying effects of erosion due to water flow blockage or narrow stream passages, and provided insights into depositional processes, like flood plain sedimentation in crevasse splay deposition or scouring processes in bends or shallow thalwegs. Also, anthropogenic actions like dumping, damming, or pilings of debris or sediment have been observed.

Our results contribute to a deeper understanding of the quantitative morphological changes triggered by the destructive flood in the Ahr Valley and highlight the benefits of Remote Sensing-based methodologies. Furthermore, they emphasize the imperative of evaluating and implementing enhanced flood mitigation measures for future flood events, as they highlight affected locations and can serve as the foundation for identifying vulnerable areas for future floods. A necessity of additional flood mitigation measures was demonstrated again by recent flood events in Germany and in light of a changing climate.

Abbreviations

B	Belgium
DTM	Digital Terrain Model
DE	Germany
DInSAR	Differential Interferometry Synthetic Aperture Radar
DoD	DTM of Difference
GCD	Geomorphonic Change Detection
LiDAR	Light Detection and Ranging
minLoD	Minimum Level of Detection
NL	The Netherlands
NRW	North Rhine-Westphalia
RP	Rhineland-Palatinate

Supplementary Information

The online version contains supplementary material available at <https://doi.org/10.1186/s12302-024-00893-x>.

Additional file 1: Figure S1. Profile A-B Area 1. **Figure S2.** Profile C-D Area 2. **Figure S3.** Profile A-B Area 3. **Figure S4.** Profile C-D Area 3. **Figure S5.** Profile A-B Area 4. **Figure S6.** Profile E-F Area 4. **Figure S7.** Profile A-B Area 5.

Acknowledgements

The authors would like to thank Janek Walk for his valuable comments on DoD calculations. The authors would like to acknowledge the DFG Project "Feasibility study to assess the pollutant load of sediments as a result of the July flood 2021 in the transition from the low mountain range to the lowland area" (Project number: 496274914).

Author contributions

VS conceptualized the manuscript. PB, BS, HS, JS, and KR contributed specific aspects to the manuscript and improved the manuscript content. All authors read and approved the final manuscript.

Funding

Open Access funding enabled and organized by Projekt DEAL.

Availability of data and materials

Not applicable.

Declarations

Ethics approval and consent to participate

Not applicable.

Consent for publication

Not applicable.

Competing interests

The authors declare no competing interests.

Author details

¹Institute of Neotectonics and Natural Hazards, RWTH Aachen University, Aachen, Germany. ²Landeserdbendienst Rheinland-Pfalz, Landesamt Für Geologie Und Bergbau Rh.-Pfalz, Emy-Roeder-Str. 5, 55129 Mainz, Germany. ³Institute for Hydraulic Engineering and Water Resources Management, RWTH Aachen University, Aachen, Germany. ⁴Institute of Applied Biogeochemistry in Geosystems, RWTH Aachen University, Aachen, Germany.

Received: 31 January 2024 Accepted: 24 March 2024

Published online: 13 April 2024

References

1. Junghänel T, Bissolli P, Daßler J, Fleckenstein R, Imbery F, Janssen W, Kaspar F, Lengfeld K, Leppelt T, Rauthe M, Rauthe-Schöch A, Rocek M, Walawender E, Weigl E (2021) Hydro-klimatologische Einordnung der Stark- und Dauerniederschläge in Teilen Deutschlands im Zusammenhang mit dem Tiefdruckgebiet „Bernad“
2. Schneider D, Gebauer P (2021) Beiträge zur Berliner Wetterkarte: Die Flutkatastrophe im Juli 2021 in Mitteleuropa aus meteorologischer Sicht:12
3. Schäfer A, Mühr B, Daniell J et al. (2021) Hochwasser Mitteleuropa, Juli 2021 (Deutschland) : 21. Juli 2021 – Bericht Nr. 1 „Nordrhein-Westfalen & Rheinland-Pfalz“. Karlsruher Institut für Technologie (KIT)
4. Kreienkamp F, Philip SY, Tradowsky JS et al. (2021) Heavy rainfall which led to severe flooding in Western Europe made more likely by climate change – World Weather Attribution. <https://www.worldweatherattribution.org/heavy-rainfall-which-led-to-severe-flooding-in-western-europe-made-more-likely-by-climate-change/>. Accessed 20 Aug 2022
5. Mohr S, Ehret U, Kunz M et al (2023) A multi-disciplinary analysis of the exceptional flood event of July 2021 in central Europe – Part 1: event description and analysis. *Nat Hazards Earth Syst Sci* 23:525–551. <https://doi.org/10.5194/nhess-23-525-2023>
6. Korswagen Eguren P, Harish S, Oetjen J et al. (2022) Post-flood field survey of the Ahr Valley (Germany). 4TU.ResearchData
7. Dietze M, Bell R, Ozturk U et al (2022) More than heavy rain turning into fast-flowing water – a landscape perspective on the 2021 Eifel floods. *Nat Hazards Earth Syst Sci* 22:1845–1856. <https://doi.org/10.5194/nhess-22-1845-2022>
8. Saadi M, Furusho-Percot C, Belleflamme A et al (2023) How uncertain are precipitation and peak flow estimates for the July 2021 flooding event? *Nat Hazards Earth Syst Sci* 23:159–177. <https://doi.org/10.5194/nhess-23-159-2023>
9. Koks EE, van Ginkel KCH, van Marle MJE et al (2022) Brief communication: critical infrastructure impacts of the 2021 mid-July western European flood event. *Nat Hazards Earth Syst Sci* 22:3831–3838. <https://doi.org/10.5194/nhess-22-3831-2022>
10. Wolf S, Stark N, Holste I et al (2024) Evaluation of the high-energy flood of mid-July 2021 as a morphologic driver in the anthropogenically developed Ahr Valley, Germany, in interaction with infrastructures. *Environ Sci Eur* 36:1–15. <https://doi.org/10.1186/s12302-024-00860-6>
11. Landesamt für Umwelt Rheinland Pfalz (2021) Erste Ergebnisse der Gewässerproben der Ahr und der Westeifel Flüsse liegen vor. <https://fu.rlp.de/de/aktuelles/detail/news/News/detail/erste-ergebnisse-der-gewaesserp-roben-der-ahr-und-der-westeifel-fluesse-liegen-vor-2/>. Accessed 25 Aug 2022
12. GDV (2021) Versicherungsschäden durch Flutkatastrophe bei rund sieben Milliarden Euro. <https://www.gdv.de/gdv/medien/medieninformationen/versicherungsschaeden-durch-flutkatastrophe-bei-rund-sieben-milliarden-euro-69800>. Accessed 20 Aug 2022
13. European Commission (2021) Emergency Response Coordination Centre (ERCC). ECHO Daily Map of 23 July 2021. <https://erccportal.jrc.ec.europa.eu/ECHO-Products/Maps#/maps/3774>. Accessed 27 Jul 2023
14. Vorogushyn S, Apel H, Kemter M et al. (2022) Analyse der Hochwassergefährdung im Ahrtal unter Berücksichtigung historischer Hochwasser. *Hydrologie und Wasserbewirtschaftung / BfG*. - 66.2022.5. - Seite 244- 254. - ISSN 1439–1783. https://doi.org/10.5675/HYWA_2022.5_2
15. Aon (2021) Global Catastrophe Recap - July 2021. Aon-Report:19
16. Khorram S, Koch FH, van der Wiele CF, Nelson SAC (2012) Remote sensing. *SpringerBriefs in space development*. Springer, Dordrecht

17. Rahman MS, Di L (2017) The state of the art of spaceborne remote sensing in flood management. *Nat Hazards* 85:1223–1248. <https://doi.org/10.1007/s11069-016-2601-9>
18. Roggenkamp T, Herget J (2014) Reconstructing peak discharges of historic floods of the river Ahr, Germany. *Erdkunde* 68:49–59. <https://doi.org/10.3112/erdkunde.2014.01.05>
19. Lehmkuhl F, Schüttrumpf H, Schwarzbauer J et al (2022) Assessment of the 2021 summer flood in Central Europe. *Environ Sci Eur*. <https://doi.org/10.1186/s12302-022-00685-1>
20. Schüttrumpf H (2021) Das Juli-Hochwasser 2021 in NRW - Ein erster Erfahrungsbericht. *Wasser Abfall* 23:14–17. <https://doi.org/10.1007/s35152-021-0665-7>
21. James LA, Hodgson ME, Ghoshal S et al (2012) Geomorphic change detection using historic maps and DEM differencing: the temporal dimension of geospatial analysis. *Geomorphology* 137:181–198. <https://doi.org/10.1016/j.geomorph.2010.10.039>
22. Wheaton JM, Brasington J, Darby SE et al (2013) Morphodynamic signatures of braiding mechanisms as expressed through change in sediment storage in a gravel-bed river. *J Geophys Res Earth Surf* 118:759–779. <https://doi.org/10.1002/jgrf.20060>
23. Williams R (2012) DEMs of difference. *Geomorphological Techniques* 2
24. Lane SN, Westaway RM, Murray Hicks D (2003) Estimation of erosion and deposition volumes in a large, gravel-bed, braided river using synoptic remote sensing. *Earth Surf Proc Land* 28:249–271. <https://doi.org/10.1002/esp.483>
25. Wheaton JM, Brasington J, Darby SE et al (2010) Accounting for uncertainty in DEMs from repeat topographic surveys: improved sediment budgets. *Earth Surf Proc Land* 35:136–156. <https://doi.org/10.1002/esp.1886>
26. Milan DJ, Heritage GL, Large AR et al (2011) Filtering spatial error from DEMs: implications for morphological change estimation. *Geomorphology* 125:160–171. <https://doi.org/10.1016/j.geomorph.2010.09.012>
27. Haffke J (2013) Persistenz und Wandel im Ahrtal Die Vermittlung einer komplexen Kulturlandschaft
28. Deutscher Wetterdienst (2021) Niederschlag: vieljährige Mittelwerte 1981 - 2010. https://www.dwd.de/DE/leistungen/klimadatendeutschland/mittelwerte/nieder_8110_fest_html.html?view=naPublication&nn=16102. Accessed 22 May 2022
29. Deutscher Wetterdienst (2022) Lufttemperatur: vieljährige Mittelwerte 1991 - 2020. https://www.dwd.de/DE/leistungen/klimadatendeutschland/mittelwerte/temp_9120_SV_html.html?view=naPublication&nn=16102. Accessed 25 Aug 2022
30. Federal Agency for Nature Conservation (2012) Landessteckbrief Ahrtal. <https://www.bfn.de/landschaftssteckbriefe/ahrtal>. Accessed 02 Aug 2022
31. MKUEM (2022) Die Ahr. <https://wasser.rlp-umwelt.de/servlet/is/1210/>. Accessed 25 Aug 2022
32. Kremer BP (2013) Die Ahr—ein echtes Kernstück der Eifel
33. Fisang R (1993) Hydrologische Betrachtung des Naturschutzgebietes „Ahrschleife bei Altenahr“ Beiträge Landespflege Rheinland-Pfalz 16:133–155
34. Rheinland-Pfalz, Landesamt für Geologie und Bergbau Online-Karte GÜK 300. <https://www.lgb-rlp.de/karten-produkte/online-karten/onlinekart-egk300.html>. Accessed 13 Jun 2023
35. Brasington J, Langham J, Rumsby B (2003) Methodological sensitivity of morphometric estimates of coarse fluvial sediment transport. *Geomorphology* 53:299–316. [https://doi.org/10.1016/S0169-555X\(02\)00320-3](https://doi.org/10.1016/S0169-555X(02)00320-3)
36. Burghardt L, Schüttrumpf H, Wolf S et al (2022) Analyse der Schäden an Brückenbauwerken in Folge des Hochwassers 2021 an der Ahr. *Wasser Abfall* 24:12–17. <https://doi.org/10.1007/s35152-022-1346-x>
37. Anderson RS, Anderson SP (2010) *Geomorphology: The mechanics and chemistry of landscapes*. Cambridge University Press, Cambridge
38. Hjulström F (1942) Studien Über Das Mäander-Problem. *Geogr Ann* 24:233–269. <https://doi.org/10.1080/20014422.1942.11880713>
39. Wheaton JM. Uncertainty in morphological sediment budgeting of rivers, University of Southampton

Publisher's Note

Springer Nature remains neutral with regard to jurisdictional claims in published maps and institutional affiliations.